the velocity sensitivity by Doppler shift of an atomic emission line. The parameter block indicates the nesting level for the calibration loop and what interval and wavelength offset to use. The other special control function is a software servo to track an ultraviolet emission line over long periods of time. This is useful to compensate for temperature drifts of the instrument structure. The design of the instrument optics allows certain detector pairs to measure different portions of the same emission line. The servo software detects and compensates for the thermal drift by maintaining constant proportions of light measured by a detector pair. The fixed position of this function is immediately before the outer loop, which controls experiment repetition.

Parallel Operation

The power consumption of the entire UVSP instrument was an important concern. Since the variable power consumption is a function of motor stepping rates, control of these rates was required. The step rate of the entire set of electromechanical functions is software limited by an end-off shift of an assigned memory word. The shift period of this word is set by a 16-ms clock interrupt. Each software device handler tests this word before commanding any device steps. If the value of the word is zero, the handler proceeds; otherwise it must wait for the timed shifts to clear the word. The word is set by each device handler to a value proportional to the device's load. While the interrupt routine continues to shift the power delay words, other software activities can proceed in parallel with this delay function.

Another form of parallel functioning was applied to processing data from dual detector experiments. Velocity information can be calculated from these measurements, but it consumes a relatively large amount of time. A speedup of the measurement processing cycle was found necessary after launch. Since no computation is required during a light measurement interval, a portion of the computer's time was unused. This unused time was used by storing the data from a measurement until the next measurement interval when the calculations are performed.

Interrupt Support

The interrupt structure has three priority levels. The highest priority level is caused by a power fail detection circuit. It may not be locked out under any condition. The second level interrupt is associated with DMA operations. The software supports this level with a minimum of overhead. Interrupt level 3 is connected to a general purpose party line. The interrupt service software polls device addresses to identify the source. Possible sources are programmable timers, fixed period clocks, wavelength drive limit switches, day-night transition logic, and others.

The software requires timing information to carry out the experiment control task. Two clock interrupts are used to supply most of the timing and synchronization information. The periods of these clocks are 16 and 64 ms. The longer period is used by the software mainly for data output synchronization. The 16-ms period matches the science data output rate for this instrument. The software uses this to control output data flow. The 16-ms event is also used to test for new SCI commands from the spacecraft. The ELU contains two programmable timers which are used for precision interval timing. These support the photomultiplier measurements and wavelength drive stepper motor motion.

Wavelength Drive Control

The wavelength drive is operated by a combination of software and hardware functions. The wavelength drive steps are triggered by a computer controlled programmable timer. The wavelength drive software controls a ramp which starts at 100 Hz and peaks at 500 Hz. This is required because the stepper motor turns a reduction gear train with significant inertia. The ramp function is defined by data from a table in memory. In addition, the software tracks a motor feedback signal to detect stepping errors. This signal is produced by optically sensing a slit on a disk fastened to the motor shaft. If the slit is not found within a preset range, the software terminates the ramp and attempts to resynchronize the motor position with the software position count.

The software directing this unit is the most time-critical function performed. During wavelength drive motion a short polling list is substituted for the level 3 interrupts to detect the minimum set of external events needed. This polling is done for a variable period of time proportional to and shorter than the motor stepping period. Between each motor step the software calculates the number of polling cycles, allowing for the maximum time required to manage the ramp and rotation tracking. When either all the polling cycles are completed or a clock event signal is detected and serviced, control proceeds to poll for a timer-triggered wavelength motor step. DMA operations function normally during wavelength motion, but software does not recognize experiment control functions from the spacecraft.

Conclusion

This discussion has covered only a portion of the features and complexity of this software. While the operational objectives did contribute to the quantity of programming, the mechanical and electronic constraints caused much of the difficulty in attaining the objectives. The greatest need was for good computer access to timing, synchronization, and device position information.

Acknowledgments

We would like to acknowledge several individuals. Kimberly Harbeck, while at the Laboratory for Atmospheric and Space Physics of the University of Colorado, developed the first generation computer software for the HRUV Spectrometer instrument. Steven A. Schoolman of Lockheed Palo Alto Research Lab provided valuable inputs to the computer operating system architecture and wrote the command generation interface software between experimenters and the instrument computer. This work was performed under NASA Contract NAS5-24119.

References

[1]Woodgate, B.E. et al., "The Ultraviolet Spectrometer and Polarimeter on the Solar Maximum Mission," *Solar Physics,* Vol. 65, Feb. 1980, p. 73.

[2]Hansen, E. and Bruner, E.C., "The University of Colorado OSO-8 Spectrometer Experiment III. Control System," *Space Science Instrument,* Vol. 5, 1979, p. 3.

AIAA 80-0083R

Helmholtz Resonator Burners: Analysis for Response Function Measurements

H.F.R. Schöyer*
Delft University of Technology, Delft, the Netherlands

Nomenclature

A_{nm} = integration constant
a = velocity of sound

Presented as Paper 80-0083 at the AIAA 18th Aerospace Sciences Meeting, Pasadena, Calif., Jan. 14-16, 1980; submitted Feb. 7, 1980; revision received Aug. 27, 1981.

*Senior Faculty Member, Department of Aerospace Engineering; Consultant, National Defense Organization TNO. Member AIAA.

B_l, C_l = integration constant
D = cavity diameter
d = diameter
F = frequency
k = complex circular frequency
L = length
L^* = characteristic length
M = Mach number
m = mass flow
O = cross-sectional area
p = pressure
R_b = response function
t = time
V = volume
v = velocity
x = coordinate
γ = ratio of specific heats
ϵ = quantity of order M
χ = dimensionless coordinate
λ = dimensionless length, wavelength
ρ = density
τ = dimensionless time

Indices and Superscripts

0 = zero-order solution
1 = primary cavity
2 = secondary cavity
l = index 1 or 2
m = cavity index, 1 or 2
n = index 1, 2, 3, or 4
$( )'$ = perturbed quantity
$\bar{( )}$ = mean quantity
$( )^i$ = imaginary part
$( )^r$ = real part
ν = neck

Introduction

THE combustion of solid rocket propellants during pressure oscillations may be characterized by the propellant response function R_b.[1] This function depends on the oscillatory frequency, mean pressure, initial propellant temperature, and propellant formulation. It is defined as

$$R_b = (m'/\bar{m})/(p'/\bar{p}) \tag{1}$$

and describes the variation of the (complex) mass production at the burning surface as a result of a (complex) pressure fluctuation.

Although numerous attempts have been made to model the propellant response function,[1-3] measurements remain necessary to obtain reliable data. The standard device to measure it is the T burner.[4] Basically this is a cylindrical tube with propellants at both ends exhausting into a pressurized surge tank. A standing wave is generated, the wavelength being about twice the T burner length. As the T burner length determines the frequency, it is a tuned device. At low frequencies, very long T burners are required. Experiments with T burners of 20 m length have been reported.[5] At such great lengths, viscous damping and heat transfer cause a nonuniform temperature and velocity distribution, leading to less reliable results. At low frequencies therefore, one has to resort to other devices, such as the L* burner.[6,7] The oscillatory frequency in an L* burner is believed to be determined by the propellant, therefore it is not a tuned device. This implies that it is almost impossible to control the L* burner in such a way that pressure oscillations of a required frequency will occur. Also other test devices, such as the rotating valve apparatus[8] and the microwave system,[9] have been developed to measure the propellant response function.

In the past, Helmholtz resonator burners (HR burners) were occasionally used for response function measurements. Price[10] briefly reports about his "Dumbbell" resonator. Recently a renewed interest has been noted.[11,12] Lyon[11] applies the HR burner to measure the velocity-coupled response function. One reason for this renewed interest is that HR burners have a smaller exposed wall surface area than T burners so that a reduction in heat losses and viscous damping may be expected. To see this, consider the double Helmholtz resonator burner (DHR burner) and the HR burner shown in Fig. 1, where some possible propellant locations have been indicated. In fact, Lyon[11] puts the propellant in the neck. It is not necessary for all of the walls to be covered with propellant.

The resonance frequency of a double Helmholtz resonator is fairly accurately[12,13] determined by considering the gas in the cavities V_1 and V_2 as being compressible and by regarding the mass of gas in the neck as a solid piston. Such an analysis predicts for the resonance frequency F,

$$F = \frac{a}{2\pi}\sqrt{\frac{\pi d_\nu^2}{4L_\nu}\left(\frac{1}{V_1}+\frac{1}{V_2}\right)} \tag{2}$$

and for the single Helmholtz resonator

$$F = \frac{a}{2\pi}\sqrt{\frac{\pi d_\nu^2}{4L_\nu}\frac{1}{V}} \tag{3}$$

The resonance frequency is determined by three geometric variables: the cavity volume(s) and the length and diameter of the neck. Comparing the exposed wall surface area of DHR and HR burners with that of the T burner at the same resonance frequency or wavelength λ is favorable for the DHR and HR burners. This is illustrated in Fig. 2 for cylindrical DHR and HR burners where only one end wall was covered with a propellant disk. These burners do not represent

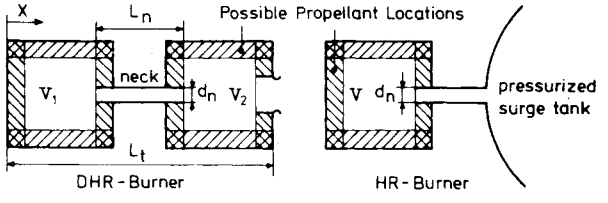

Fig. 1 Diagram and nomenclature for Helmholtz resonator burners.

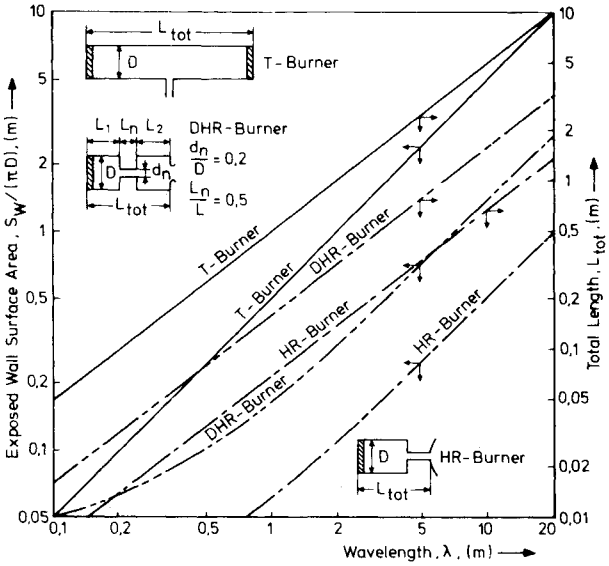

Fig. 2 Exposed wall surface area and total length for HR, DHR, and T burners in relation to the oscillatory wavelength.

an optimum, the example merely illustrates the reduction in the exposed cold wall surface area. At large wavelengths, i.e., at low frequencies, the total length of DHR and HR burners is reduced considerably as compared to the T burner. This makes Helmholtz resonators attractive instruments for response function measurements.

Elementary Analysis

Consideration of inviscid and one-dimensional flow and isentropic oscillations reveals the basic acoustics of (D)HR burners, although in practice there is heat transfer and wall friction in the neck does have an appreciable effect.[13,14] The response of a supersonic nozzle in the case of a (D)HR burner may be estimated by the usual "zero-length" approximation

$$v'/\bar{v} = [(\gamma-1)/(2\gamma)]\,(p'/\bar{p}) \tag{4}$$

The propellant response R_b has been defined as

$$R_b = (m'/\bar{m})/(p'/\bar{p}) = [\rho'/\bar{\rho} + v'/\bar{v}]/(p'/\bar{p}) \tag{5}$$

The boundary condition at the propellant is:

$$v'/\bar{v} = (R_b - 1/\gamma)\,(p'/\bar{p}) \tag{6}$$

The wave equation, describing the pressure oscillations in the cavities and the neck, accounting for a (small) mean flow component $\bar{v}$ is

$$p'_{tt} + 2\bar{v}p'_{xt} + (\bar{v}^2 - \bar{a}^2)p'_{xx} = 0 \tag{7}$$

Introducing the dimensionless variables

$$\tau = kt \tag{8}$$

and

$$\chi = kx/\bar{a} \tag{9}$$

yields the wave equation

$$p'_{\tau\tau} + 2Mp'_{\tau\chi} + (M^2-1)p'_{\chi\chi} = 0 \tag{10}$$

The general solution of the wave equation for cavity m is

$$\begin{aligned} p'_m = {} & A_{1m}\exp\{i[\tau(1+M_m)-\chi]\} \\ & + A_{2m}\exp\{-i[\tau(1+M_m)-\chi]\} + A_{3m} \\ & \times\exp\{i[\tau(1-M_m)+\chi]\} + A_{4m}\exp\{-i[\tau(1-M_m)+\chi]\} \end{aligned} \tag{11}$$

This solution holds for both cavities and for the neck. The constants A_{nm} follow from the boundary conditions and match the flow in the cavities and the neck. The boundary conditions at the burning surface in the primary cavity yield

$$\begin{aligned} A_{31} &= A_{11}[1 - 2M_1(\gamma R_b - 1 + i\tau)] \\ A_{41} &= A_{21}[1 - 2M_1(\gamma R_b - 1 + i\tau)] \end{aligned} \tag{12}$$

where terms of order M^2 and higher have been neglected.

The boundary conditions at the nozzle yield

$$\begin{aligned} A_{32} &= A_{12}\left[1 - 2M_2\left(\frac{\gamma-1}{2} - i\tau\right)\right]\exp(-2i\lambda_t) \\ A_{42} &= A_{22}\left[1 - 2M_2\left(\frac{\gamma-1}{2} - i\tau\right)\right]\exp(2i\lambda_t) \end{aligned} \tag{13}$$

where λ_t is the nondimensional total length of the DHR burner. The velocity and pressure fluctuations in the cavities adjacent to the neck must match the fluctuations at the neck ends.

Although, the wave equation for the neck may be solved, the gas in the neck may also be regarded as a "solid piston," simplifying the analysis without introducing unacceptably large errors.[13] In this way, one also neglects the effects of flow contraction and expansion near the neck ends. To accommodate for these effects, end corrections may be applied.[14] Matching the flow at the neck ends with the flow in the cavities yields

$$v'_m/v'_v = \bar{v}_m/\bar{v}_v = O_v/O_m \tag{14}$$

For a DHR burner, one then obtains

$$\begin{aligned} & O_l A_{l1}\{i\sin\lambda_l + (-1)^l M_l[(\gamma R_b - 1)\exp\{i^{(2l-1)}\lambda_l\} \\ & \quad + \tau\sin\lambda_l]\} = O_2 A_{l2}\exp\{i^{(2l+1)}\lambda_t\}\left[-i\sin\lambda_2 + (-1)^l \right. \\ & \quad \left. \times M_2\left\{\frac{\gamma-3}{2}\exp(i^{(2l+1)}\lambda_2) - \tau\sin\lambda_2\right\}\right] \end{aligned} \tag{15}$$

for $l = 1, 2$.

The equation of motion for the piston of gas in the neck provides a third relation between the constants A_{lm}

$$\begin{aligned} & \frac{\lambda_v O_2}{O_v}\sum_{m=1}^{2} A_{2m}\exp[i^{(2m-1)}(\tau - \lambda_t)]\left\{-\sin\lambda_2 + i^{(2m-1)}\right. \\ & \quad \left. \times M_2\left[\frac{\gamma-3}{2}\exp(-i\lambda_2) - \tau\sin\lambda_2 + i^{(2m-1)}\sin\lambda_2\right]\right\} \\ & \quad = \sum_{m=1}^{2}\sum_{l=1}^{2}(-1)^m A_{lm}\exp\{i^{(l-1)}[\tau - (m-1)\lambda_t]\} \\ & \quad \times\left\{\cos\lambda_m - M_m\left[\left\{(\gamma R_b - 1)(2-m) - \frac{\gamma-1}{2}(1-m)\right\}\right.\right. \\ & \quad \left.\left. \times\exp\{i^{(2l+1)}\lambda_m\} - i^{(2l+1)}\tau\cos\lambda_m\right]\right\} \end{aligned} \tag{16}$$

Replacing the circular frequency k by $-k$, λ by $-\lambda$, and τ by $-\tau$ interchanges the constants A_{1m} and A_{2m} in Eq. (16). Therefore, it suffices to analyze those parts of Eq. (16) that are multiplied by $\exp(i\tau)$. As in all cases, the dimensions of the burners are small compared to the wavelength, $\sin\lambda \approx \lambda_m$ and $\cos\lambda_m \approx 1$. Equation (15) then yields

$$A_{11} = \frac{O_2 A_{12}}{O_1}\exp(-i\lambda_t)\left(\frac{-\lambda_2 + iM_2(\gamma - 3/2 - \tau\lambda_2)}{\lambda_1 + iM_1[(\gamma R_b - 1) + \tau\lambda_1]}\right) \tag{17}$$

Inserting this result into the appropriate part of Eq. (16) yields the equation for the complex circular frequency of the possible oscillations in the DHR burner

$$\begin{aligned} & \frac{\lambda_v}{O_v}\left[-\lambda_1\lambda_2 - i\lambda_2 M_1(\gamma R_b - 1 + \tau\lambda_1)\right. \\ & \quad \left. + i\lambda_1 M_2\left(\frac{\gamma-3}{2} - \tau\lambda_2 + i\lambda_2\right)\right]\frac{1}{O_1}\left[-\lambda_2 + \lambda_2 M_1\right. \\ & \quad \left. \times(\gamma R_b - 1 - i\tau) + iM_2\left(\frac{\gamma-3}{2} - \tau\lambda_2\right)\right] \\ & \quad - \frac{1}{O_2}\left[\lambda_1 - \lambda_1 M_2\left(\frac{\gamma-1}{2} - i\tau\right) + iM_1(\gamma R_b - 1 + \tau\lambda_1)\right] \end{aligned} \tag{18}$$

Substituting $\lambda = Lk/a$ and $\tau = kt$ yields a fourth-order algebraic equation in the complex frequency k

$$\epsilon_1 k^4 + (\epsilon_2 - A)k^3 + \epsilon_3 k^2 + (\epsilon_4 + B)k + \epsilon_5 = 0 \tag{19}$$

All coefficients ϵ are of the order M_1 and/or M_2 and are therefore small. The coefficients A and B stand for

$$A = L_v/(O_v a^3) \tag{20}$$

$$B = (1/V_1 + 1/V_2)/a \tag{21}$$

The zero-order solution of Eq. (19) hence is:

$$k_0 = a\sqrt{O_v(1/V_1 + 1/V_2)/L_v} \tag{22}$$

corresponding to the well-known classical solutions, Eqs. (2) and (3). In addition

$$\epsilon_1 = -itL_v(M_1 + M_2)/(O_v a^3)$$

$$\epsilon_2 = L_v M_2/(O_v a^3)$$

$$\epsilon_3 = iL_v[M_2(\gamma-3)/(2L_2) - M_1(\gamma R_b - 1)/L_1] \div O_v a^2) + it(M_1 + M_2)(1/V_1 + 1/V_2)/a$$

$$\epsilon_4 = -M_1(\gamma R_b - 1)/(aV_1) - M_2(\gamma - 1)/(2aV_2)$$

$$\epsilon_5 = i\{M_1(\gamma R_b - 1)/(L_1 V_2) - M_2(\gamma - 3)/(2L_2 V_1)\} \tag{23}$$

Writing $k = k_0 + k'$, where $|k'| \ll |k|$ and subsequent substitution of this relation into Eq. (19) yields the frequency perturbation, due to the presence of burning propellant and a nozzle

$$\frac{k'}{k_0} = \frac{i}{2}\left(\frac{a}{k_0 L_2}\frac{\gamma-3}{2}\frac{M_2 V_1}{V_1+V_2} + \frac{a}{k_0 L_1}(\gamma R_b - 1)\frac{M_1 V_2}{V_1+V_2}\right) + \frac{1}{2}\left(-\frac{M_1 V_2}{V_1+V_2}(\gamma R_b - 1) - \frac{M_2 V_1}{V_1+V_2}\frac{\gamma-3}{2}\right) \tag{24}$$

Usually, the terms in the first bracket of Eq. (24) dominate; for example, with $d_v/D = 0{,}2$ and $L_1 = L_2 = 2L_v$, $a/(k_0 L) \approx 50$ and by good approximation

$$k' = \frac{ia}{2}\left(\frac{(\gamma R_b - 1)M_1 V_2}{L_1(V_1+V_2)} - \frac{3-\gamma}{2}\frac{M_2 V_1}{L_2(V_1+V_2)}\right) \tag{25a}$$

or, if the HR burner is connected to a large surge tank

$$k' = \frac{ia}{2}\frac{M_1}{L}(\gamma R_b - 1) \tag{25b}$$

The real and imaginary parts of the frequency perturbation hence are

$$k'^{(r)} = \frac{\gamma a R_b^{(i)}}{2L_1}\frac{M_1}{1+V_1/V_2} \tag{26a}$$

$$k'^{(i)} = \frac{a}{2}\frac{(\gamma R_b^{(r)} - 1)}{L_1(1+V_1/V_2)} - \frac{3-\gamma}{L_1}\frac{aM_2}{L_2}\frac{V_1/V_2}{1+V_1/V_2} \tag{26b}$$

The real part of the frequency perturbation causes a (small) frequency shift and the imaginary part causes growing or decaying amplitudes. The (complex) pressure at a fixed position in the burner is, according to Eq. (11)

$$p' = B_1 e^{-ikt} + B_2 e^{+ikt}$$

During experiments, one measures the real part of the pressure. Writing $k = k^{(r)} + ik^{(i)}$ it is obvious that the measured pressure perturbation in a DHR burner may be expressed as

$$p' = C_1 \cos(k^{(r)} t)\exp\left(\frac{aM_1}{2L_1}\frac{(\gamma R_b^{(r)} - 1)}{1+V_1/V_2} - \frac{3-\gamma}{4}\frac{aM_2}{L_2}\frac{V_1/V_2}{1+V_1/V_2}\right)t \tag{27a}$$

For an HR burner, venting into a large surge tank, one finds

$$p' = C_2 \cos(k^{(r)} t)\exp\left(\frac{aM_1}{2L_1}(\gamma R_b^{(r)} - 1)\right)t \tag{27b}$$

which is analogous to what is obtained in T burner analyses. If no spontaneous oscillations occur, pressure oscillations may be created by pulsing the burner. From the logarithm of the amplitude history, the real part of the propellant response function may then be obtained

$$R_b^{(r)} = \frac{1}{\gamma} + \frac{L_1}{M_1}\left(\frac{2(1+V_1/V_2)\ln[\hat{p}'(t_2)/\hat{p}'(t_1)]}{\gamma a(t_2 - t_1)} + \frac{3-\gamma}{2\gamma}\frac{M_2}{L_2}\frac{V_1}{V_2}\right) \tag{28a}$$

for the DHR burner, and

$$R_b^r = \frac{1}{\gamma} + \frac{L_1}{M_1}\left(\frac{2\ln[\hat{p}'(t_2)/\hat{p}'(t_1)]}{\gamma a(t_2 - t_1)}\right) \tag{28b}$$

for an HR burner venting into a large surge tank.

Conclusions

The concept of Helmholtz resonator-type burners is simple and, according to the above analysis, the devices are suitable for measuring the real part of the response function of solid propellants. To extract this information from experimental data, a data-reduction procedure can be applied which is similar to that for T burner data reduction.

If no spontaneous oscillations occur, the HR burner may be pulsed; from the decay of the resulting amplitudes, the response function can be determined. Advantages are that HR burners are tuned and that even at very low resonant frequencies the dimensions remain small, reducing heat-transfer and viscosity effects. In addition, HR burners can use many existing T burner components, such as the surge tank and tubes.

It is clear that an HR burner, venting into a surge tank is the more advantageous concept, as the nozzle damping term is eliminated. However, it has already been shown experimentally by Lyon[11] that DHR burners with a nozzle also allow for response function measurements. It should be mentioned that many variations of HR-type burners are possible.

At the Department of Aerospace Engineering of Delft University of Technology a small experimental program is presently being conducted to investigate the merits and disadvantages of HR-type burners.

References

[1] Culick, F.E.C., "A Review of Calculations for Unsteady Burning of a Solid Propellant," *AIAA Journal*, Vol. 6, Dec. 1968, pp. 2241-2255.

[2] Brown, R.S. and Muzzy, R.J., "Linear and Nonlinear Pressure Coupled Combustion Instability of Solid Propellants," *AIAA Journal*, Vol. 8, Aug. 1970, pp. 1492-1500.

[3] Cohen, N.S., "Response Function Theories that Account for Size Distribution Effects—A Review," AIAA Paper 80-1125, June-July 1980.

[4] Culick, F.E.C. et al., "T-Burner Manual," Chemical Propulsion and Information Agency, Silver Spring, Md., CPIA Pub. 191, 1969.

[5]Eisel, J.L., Horton, M.D., Price, E.W., and Rice, D.W., "Preferred Frequency Oscillatory Combustion of Solid Propellants," *AIAA Journal,* Vol. 2, July 1964, pp. 1319-1323.

[6]Beckstead, M.W. and Price, E.W., "Nonacoustic Combustor Instability," *AIAA Journal,* Vol. 5, Nov. 1967, pp. 1989-1996.

[7]Schöyer, H.F.R., "Results of Experimental Investigations of the L* Phenomenon," *Journal of Spacecraft and Rockets,* Vol. 17, May-June 1980, pp. 200-207.

[8]Brown, R.S. and Waugh, R.C., "Pressure and Velocity Response Function Measurements by the Rotating Valve Method," *Solid Rocket Motor Technology,* AGARD Conference Proceedings No. 259, Technical Editing and Reproduction Ltd., London, 1979.

[9]Strand, L.D. and McNamara, R.P., "A Variable-Frequency Driver-Microwave Transient Regression Rate Measurement System," *Progress in Astronautics and Aeronautics: Experimental Diagnostics in Combustion of Solids,* edited by T.L. Boggs and B.T. Zinn, Vol. 63, AIAA, New York, 1978.

[10]Price, E.W., "Experimental Measurements in Solid Propellant Rocket Combustion Instability," Sec. 3, "Methods for Studying Combustor Parts," *Experimental Methods in Combustion Research,* AGARD-NATO, Paris, 1964.

[11]Lyon, J.M. and Crump, J.E., "Use of a Helmholtz Burner for Low Frequency Velocity Coupled Instability Measurements," Paper presented at the 17th JANNAF Combustion Meeting, 1980.

[12]Schöyer, H.F.R., "The Helmholtz Resonator as a Tool for Low-Frequency Combustion Research," AIAA Paper 80-0083, Jan. 1980.

[13]DeGroot, W.A., "The Helmholtz Resonator: Analysis and Experiments," Engineering Thesis, Delft University of Technology, Dept. of Aerospace Engineering, Delft, the Netherlands, Sept. 1980.

[14]Ingard, U., "On the Theory and Design of Acoustic Resonators," *The Journal of the Acoustical Society of America,* Vol. 35, Nov. 1953, pp. 1037-1067.